IOP Publishing Nanotechnology
Nanotechnology **28** (2017) 385101 (11pp) https://doi.org/10.1088/1361-6528/aa7f84

Functionalization of nanotextured substrates for enhanced identification of metastatic breast cancer cells

Nuzhat Mansur[1,2,3], Mohammad Raziul Hasan[1,2,3], Young-tae Kim[3,4] and Samir M Iqbal[1,2,3,4,5]

[1] Nano-Bio Lab, University of Texas at Arlington, Arlington, Texas 76019, United States of America
[2] Department of Electrical Engineering, University of Texas at Arlington, Arlington, Texas 76019, United States of America
[3] Nanotechnology Research Center, University of Texas at Arlington, Arlington, Texas 76019, United States of America
[4] Department of Bioengineering, University of Texas at Arlington, Arlington, Texas 76019, United States of America
[5] Department of Urology, University of Texas Southwestern Medical Center at Dallas, Dallas, Texas 75235, United States of America

E-mail: SMIQBAL@uta.edu

Received 4 June 2017, revised 12 July 2017
Accepted for publication 13 July 2017
Published 1 September 2017

Abstract

Metastasis is the major cause of low survival rates among cancer patients. Once cancer cells metastasize, it is extremely difficult to contain the disease. We report on a nanotextured platform for enhanced detection of metastatic cells. We captured metastatic (MDA-MDB-231) and non-metastatic (MCF-7) breast cancer cells on anti-EGFR aptamer modified plane and nanotextured substrates. Metastatic cells were seen to change their morphology at higher rates when captured on nanotextured substrates than on plane substrates. Analysis showed statistically different morphological behaviors of metastatic cells that were very pronounced on the nanotextured substrates. Several distance matrices were calculated to quantify the dissimilarity of cell shape change. Nanotexturing increased the dissimilarity of the metastatic cells and as a result the contrast between metastatic and non-metastatic cells increased. Jaccard distance measurements found that the shape change ratio of the non-metastatic and metastatic cells was enhanced from 1:1.01 to 1:1.81, going from plane to nanotextured substrates. The shape change ratio of the non-metastatic to metastatic cells improved from 1:1.48 to 1:2.19 for the Hausdorff distance and from 1:1.87 to 1:4.69 for the Mahalanobis distance after introducing nanotexture. Distance matrix analysis showed that nanotexture increased the shape change ratios of non-metastatic and metastatic cells. Hence, the detectability of metastatic cells increased. These calculated matrices provided clear and explicit measures to discriminate single cells for their metastatic state on functional nanotextured substrates.

Keywords: nanotexture, metastatic breast cancer, distance matrix analysis, Jaccard distance, Hausdorff distance, Mahalanobis distance, cell cytology

(Some figures may appear in colour only in the online journal)

1. Introduction

Cancer occurs when some of the cells start dividing uncontrollably and spread into surrounding tissues. Cancer can start in almost any organ of our body. It is among the leading causes of mortality and morbidity. According to the World Cancer Report, in 2014, approximately 14.1 million new cancer cases were reported while 6.2 million people died [1].

Over the next two decades, the number of new cases are expected to increase by about 70%. Cancer metastasis is the chief cause for cancer related deaths. During the metastasis process, metastatic cells start to spread to other organs by penetrating surrounding tissues and then invading blood. The stages of metastasis include the invasion of cancer cells to adjacent tissues, intravasation or cell movement through the walls of nearby blood vessels, transport of metastatic cells through circulatory system, arresting of those cells at secondary sites, and extravasation or invasion to secondary sites for growth [2, 3]. When metastatic cells reach distant organs and start creating new tumors there, it is called stage IV or the last stage of cancer. Most types of metastatic cancers are still incurable with current treatments and technologies. In some cases, treatments can prolong life, but 90% of cancer related deaths are caused by metastasis [4]. It is important to detect metastatic cancer at very early stages. Early detection here has been used from the point of view of detecting metastatic cancer cells either from a biopsy tissue of the originating site or peripheral blood before they establish a distant tumor in other organs and create stage IV cancer. Early detection can enable stage-specific treatment and care which can increase survival rate and improve the quality of life.

Many studies have been reported on the detection and isolation of cancer cells. Most studies used microfluidic devices where the cells flow through and interact with physical or chemical cues. Nagrath *et al* reported a microfluidic device to collect circulating tumor cells from peripheral blood using EpCAM specific antibody coated microposts [5]. Adams *et al* developed a polymer based microfluidic device with an antibody coated surface to capture metastatic breast cancer cells from blood [6]. Tan *et al* demonstrated a label-free microfluidic device to isolate cancer cells based on their physical deformability and size [7]. Among the labeled detection schemes, Swennenhuis *et al* characterized metastatic prostate cancer cells by fluorescence *in situ* hybridization [8]. A large number of these reports used an affinity based interaction between cell membrane proteins and ligands to isolate cancer cells. Affinity based interaction is highly selective and specific. Aptamers have also been used for affinity based detection [9]. It has been reported that aptamers work better than antibodies [10]. Aptamers are highly stable in various salt and ionic conditions and can be precisely immobilized on specific sites. They can be reversibly denatured [11]. Aptamers are preferred over antibodies in detecting cancer cells due to such flexibility in probe design.

Nanotextured substrates are the emerging biosensing platforms to capture or isolate cancer cells. Nanotexture increases the effective surface area of substrates and augments sensitivity, but the tradeoff is specificity. This problem is overcome by introducing specific antibodies and aptamers. The idea of introducing nanotexture into device design comes from nature. Micro or nanoscale structures are vastly seen in plants, insects, and even in human tissues. The vascular endothelial basement membranes in the human body have 3D nanoscale topography. This kind of structure influences cellular functions significantly [12]. Cancer cells anchor to basement membranes using cell adhesion molecules and invade the barrier [13]. Nanoscale structures provide higher interactions with biomolecules, which is a primary requirement for any sensing technique. The sensing devices often use defined nanotopography for cell capture [5]. To study cell morphology, adhesion, and migration, Fischer *et al* used micro and nanoscaled array of silicon pillars [14]. To separate T lymphocyte, 100–200 nm sized silicon nanowires functionalized with streptavidin were used. The resulting capture efficiency was 88% [15]. We previously reported the synthesis of a biocompatible scaffold from nanotextured chicken eggshell [16]. Such nanotextured scaffolds can remarkably increase the density of some cells [17, 18]. Previously, we fabricated random nanotopography on substrates that could selectively capture 93% of cancer cells when functionalized with an aptamer [19–22]. Morphological changes in brain cancer cells on these substrates have also been reported by our group [9, 23]. Our platform was simple and easy to fabricate. Use of aptamers provided higher selectivity and specificity against epidermal growth factor receptors (EGFRs) of cell membranes.

EGFR is the most frequently overexpressed membrane receptor tyrosine kinase oncogene [24–26]. In benign breast cancer cells, the EGFR expression is 1.5×10^4 receptors/cell whereas in metastatic breast cancer cells it is 1.3×10^5 receptors/cell, a ten-fold increase [27, 28]. Using this differential expression, we report measurements of differential morphology of metastatic and non-metastatic breast cancer cells on anti-EGFR aptamer coated plane and nanotextured substrates. This modality can be used to define the metastatic grade of a given sample whether the cells come from a biopsy sample or are collected from blood (e.g. circulating tumor cells). In this work, we introduced nanotexture into our platform. Nanotexturing modulated and amplified the activity of captured cancer cells. The effect was much more pronounced for metastatic breast cancer cells. These cells changed their shapes rapidly on nanotextured substrates distinguishing them from non-metastatic cells. A number of quantitative features were developed to clearly identify metastatic breast cancer cells.

2. Materials and methods

All chemicals used in the experiments were obtained from Sigma-Aldrich (St. Louis, MO, USA), unless mentioned otherwise.

2.1. Substrate preparation

Fisher brand microscope slides (12-550D, Fisher Scientific) were cut into 5 mm × 5 mm pieces and used as substrates. Two types of substrates were used. One type was just plane untreated microscope glass slides. The second type consisted of nanotextured slides, produced by reactive ion etching (RIE). A Technics Micro-RIE Series 800 Plasma System was used to do the RIE. A gas mixture of 10 sccm O_2 and 15 sccm

of CF_4 was used in RIE for 25 min to create the nanotexture. The RF power was set at 200 W during the RIE. Nanotextured substrates were marked to easily separate them from the plane ones.

2.2. Substrate characterization

2.2.1. Topography examination. Roughness was measured by atomic force microscope (AFM). Non-contact AFM mode was used (Park XE70 AFM) to collect the topographical data. The maximum tip diameter was less than 10 nm. The nominal force constant and resonance frequency were 42 N m^{-1} and 330 kHz, respectively. Five samples for each type of substrate were scanned and plane leveled. The average, RMS roughness, and maximum peak to valley height were measured.

A Hitachi S-3000N variable pressure scanning electron microscope (SEM) was used to examine the surfaces of the nanotextured substrates. The substrates were coated with 5 nm gold film and an acceleration voltage of 18 kV was used to capture micrographs.

2.2.2. Elemental analysis. Elemental analysis of the substrates was done with the energy-dispersive x-ray spectroscopy (EDS) tool of the SEM. It quantified the elemental composition of the substrates at low vacuum and 30 kV acceleration voltage.

2.2.3. Contact angle measurements. The contact angles of the plane and nanotextured substrates were measured with a Ramé-Hart contact angle goniometer (NRL-100; Ramé-hart Instrument Co, NJ, USA). Deionized (DI) water sessile drops were placed on the substrates at room temperature and contact angles were visually observed through a microscope at the water-substrate interface. Five measurements were taken for each of the total of seven runs.

2.3. Substrate functionalization

All substrates were cleaned with Piranha solution (H_2SO_4:H_2O_2::3:1). This process created –OH groups on the surface. A 200 μl solution of 2% (3-aminopropyl)triethoxysilane (APTES) in ethanol was used to create amine groups on the surface. A solution of 9 ml dimethyl sulfoxide (DMSO), 1 ml pyridine and 0.002 gm of *p*-phenylene diisothiocyanate (PDITC), was prepared and the substrates were immersed in it. To cap unreacted PDITC groups, a solution of 150 mmol l^{-1} N,N-diisopropylethylamine (DIPEA) in dimethylformamide (DMF) and 50 mmol/l 6-amino-1-hexanol was used. The diisothiocyanate layer created by PDITC was chemically bound with the surface-tethered APTES. The other end of the layer was capable of binding with an amine-bearing single-stranded DNA (ssDNA) molecule. The ssDNA molecules were suspended in DMSO and 20 μl of 5 μM ssDNA solution was placed on each of the substrates. The substrates were incubated for 18 h at 45 °C.

2.4. Aptamer preparation and substrate functionalization with aptamer

Aptamer isolation and synthesis have been described elsewhere [29]. Briefly, the anti-EGFR RNA aptamer was isolated from a pool of 62-nucleotide random region using a method called SELEX. It was isolated by iteratively selecting binding species against purified human EGFR (R&D Systems, Minneapolis, MN, USA). The high affinity (K_d = 2.4 nmol/l) aptamer was synthesized in-house. It was extended with a nonfunctional and scrambled capture sequence for hybridization with surface-bound ssDNA bound on the substrate. The capture sequence did not disrupt the aptamer secondary structures. The aptamer sequence was 5′-GGC GCU CCG ACC UUA GUC UCU GUG CCG CUA UAA UGC ACG GAU UUA AUC GCC GUA GAA AAG CAU GUC AAA GCC GGA ACC GUG UAG CAC AGC AGA GAA UUA AAU GCC CGC CAU GAC CAG-3′ [9]. The underlined part is the capture sequence.

Durascribe kits (Epicentre Biotechnologies, Madison, WI, USA) were used to transcribe anti-EGFR aptamer from a double-stranded DNA template. The DNA template was PCR amplified, ethanol precipitated, and mixed with reaction buffer, DTT, ATP, GTP, 2′ F-CTP, 2′ F-UTP, and a mutant T7 polymerase for 10 h at 37 °C. DNase treatment was used for 30 min at 37 °C to degrade the DNA template. An anti-EGFR aptamer was purified on an 8% denaturing PAGE. UV shadowing was used to visualize the band for the aptamer. The aptamer was excised and eluted in 0.3 mol l^{-1} sodium acetate (pH 5.2) overnight at 37 °C and ethanol precipitated. The pellet was dissolved in water. The concentration was measured on a NanoDrop spectrophotometer (Thermo Fisher Scientific, Waltham, MA USA). The aptamer was modified by extending the DNA template at its 3′ end with a 24-nucleotide sequence tag. [29].

Anti-EGFR aptamer was mixed with DEPC-treated DI water and hybridization buffer (RNA:hybridization buffer::5:1). 25 μl of 0.2 μM aptamer was placed on each substrate and incubated at 37 °C for 1 h. The substrates were later washed with 1× phosphate buffered saline (PBS) solution (pH 7.5).

2.5. Target cell preparation

Two types of breast cancer cells were used: metastatic MDA-MDB-231 and non-metastatic MCF-7. Both were obtained from the University of Texas Southwestern Medical Center at Dallas, Texas. The cells were cultured in Dulbecco's modified Eagle's medium (DMEM/F-12; Cellgro, Corning, Manassas, VA, USA) with 10% heat inactivated fetal bovine serum. L-glutamine and gentamycin were added to the medium. A sterile humidified environment was maintained (95% air, 5% CO_2 at 37 °C). Cultured cells were centrifuged, cell pellet was collected, diluted with sterilized warm 1× PBS and used immediately.

Table 1. Substrate roughness from AFM.

Substrate	Average roughness (nm) ± S.D.	RMS roughness (nm) ± S.D.	Maximum peak to valley height (nm) ± S.D.
Plane	5.76 ± 4.03	6.87 ± 3.3	28.11 ± 12.2
Nanotextured	29.75 ± 4.57	36 ± 4.9	134.5 ± 13.3

2.6. Cell suspension and image capture

Around 200 000 cells were present in 1 ml of PBS. A volume of 30 μl of cell solution was loaded on a substrate. Five minutes were given for the cells to interact with aptamer modified substrates. The cells were then tracked and imaged with optical microscope for 15 min.

2.7. Image analysis and data interpretation

Captured images were saved and processed with a MATLAB script. For each cell, an array of images showed its morphological change over 15 min. The RGB images were converted into binary images using filters and edge detector modules. Morphological changes were measured from binary images and fitted into mathematical models. The models calculated distance matrices. The output of these models showed statistically significant differences between metastatic and non-metastatic cells on nanotextured aptamer functionalized substrates.

2.8. Distance matrix analysis

2.8.1. Jaccard distance. We compared cell shapes over time and defined distance analysis and shape dissimilarity matrices to objectively detect shape change of cells. Distance matrix analysis is a standard pattern recognition technique. This technique computes shape change and presents a distance value. Distance value represents shape dissimilarity. Usually the higher the distance value, the more the shape is changing. We converted optical images into binary images having only one of two values: a black pixel or a white one. A black pixel denoted the presence of cell body at those coordinates and white denoted absence. A 2X2 contingency table was generated for each pixel. There were four conditions in the table that were derived from the presence of a cell in any two consecutive images. An '*a*' meant presence in both images. The '*b*' depicted presence in the first image but absence in next image. The '*c*' was absence in the first image and presence in next image, and absence in both images was recorded as a '*d*'. For a particular pixel, only one of the four conditions had to be true. Using this table, a distance matrix called the Jaccard distance was calculated. The Jaccard distance is calculated as [30]:

$$\text{Jaccard distance} = 1 - \frac{a}{a+b+c}.$$

2.8.2. Hausdorff distance. We calculated another distance matrix called the Hausdorff distance [31]. This matrix determined the resemblance of one point set in one image to another point set in another image. If A and B are the sets of points on a cell contour in two consecutive images, the Hausdorff distance is calculated as:

$$H(A, B) = \max(h(A, B), h(B, A))$$

where, $h(A, B) = \max_{a \in A} \min_{b \in B} |a - b|$.

2.8.3. Mahalanobis distance. Metastatic cells were seen to change cell contour continuously. Data points from the cell contour were thus always changing their distance from the initial cell boundary. The Mahalanobis distance is another distance matrix that measures the number of standard deviations that the cell periphery is away from the mean cell boundary [32]. It is calculated as:

$$D^2 = (x - m)^T C^{-1} (x - m)$$

where, D = Mahalanobis distance, m = vector of mean values from initial cell boundary, x = vector of changing cell boundary, C^{-1} = inverse covariance matrix of initial cell boundary, and T = transpose vector.

2.9. Statistical analysis with distance values

Change in distance values were calculated between two following time points for each cell. At the end of 15 min all the changes were summed up to find the total distance change for each cell. The average of total distance indicated how the group (metastatic or non-metastatic cells) behaved in terms of morphological change after 15 min. A two-tailed *t*-test was used to assess if the averages of any two groups were statistically significant. We calculated *p*-values in each case. We calculated the cell shape change ratio using the following formula:

$$\begin{aligned} &\textit{Cell shape change ratio}_{(\textit{distance},\textit{substrate})} \\ &= \textit{distance}_{\text{Jaccard }|\text{Hausdorff }|\text{Mahalanobis}} \text{ of} \\ &\textit{non} - \textit{metastatic cells}_{\textit{substrate}} / \\ &\textit{distance}_{\text{Jaccard }|\text{Hausdorff }|\text{Mahalanobis}} \text{ of} \\ &\textit{metastatic cells}_{\textit{substrate}} \end{aligned}$$

where *distance* was either the Jaccard distance or Hausdorff distance or Mahalanobis distance, and the *substrate* was either a plane or nanotextured substrate.

3. Results and discussion

3.1. Substrate topography examination

Roughness values for plane and nanotextured substrates are presented in table 1. The AFM micrograph in figures 1(a) and (b) shows surface features of both types of substrates. On

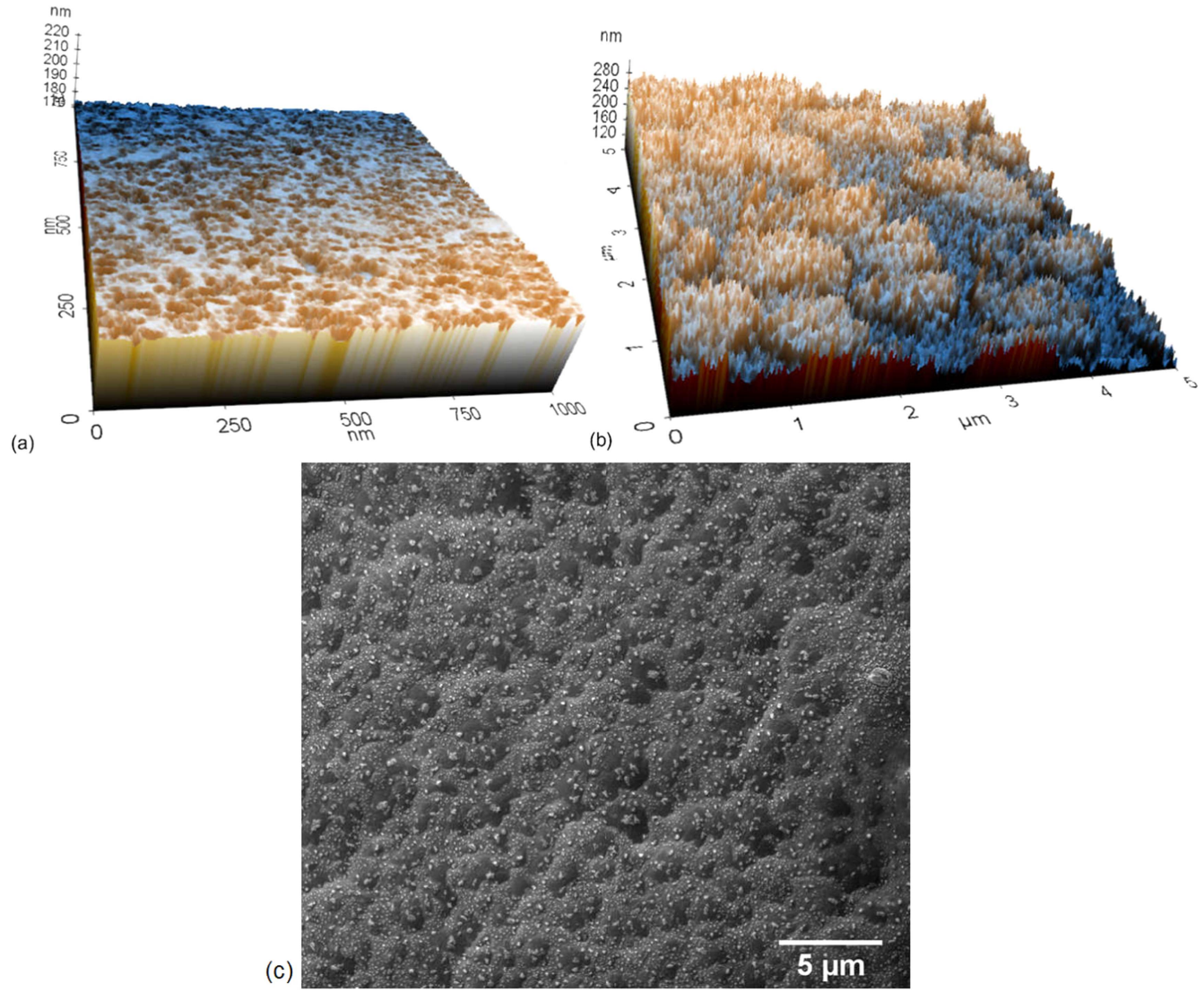

Figure 1. AFM micrographs of (a) plane substrate before RIE, (b) nanotextured substrate after RIE. (c) SEM micrograph of the nanotextured substrate.

average, nanotexturing increased the RMS roughness from ~6.8 nm (S.D. = 3.3 nm) to ~36 nm (S.D. = 4.9 nm). Increased roughness directly affected and amplified density of immobilized surface-tethered ssDNA and anti-EGFR aptamer on nanotextured substrates [15]. SEM micrograph of nanotextured substrate is shown in figure 1(c).

3.2. Elemental analysis of substrates

Elemental analysis of the plane and nanotextured substrates showed that there was no change in the composition of the substrates after RIE (figure 2). This eliminated any possible effects on cell behavior due to elemental changes. Trace amounts of C, Al, and K were found on both substrates, which were typical and came from sample handling.

3.3. Contact angle measurements

Contact angle data showed that the substrates became more hydrophilic after nanotexturing (table 2). Hydrophilic substrates are ideal for biological molecule adhesion [33]. Hydrophobic substrates deter cell attachment while hydrophilic substrates permit and even boost attachment [34–39]. Hydrophilicity is also known to enhance interaction between cell membrane and surface [35, 37]. Increased hydrophilicity of nanotextured surface thus indeed had an effect on the morphology changes of the cells. Contact angle values shown in table 2 manifest that nanotexturing increased hydrophilic behavior of the substrates and enhanced interactions between substrates and cells. The morphological changes in metastatic cells were prominent on the nanotextured substrate due to increased aptamer concentration on the nanotextured substrate, higher interaction between aptamer and cell membrane, and higher hydrophilicity [9].

3.4. Cell morphology observations

The cells were not washed from the substrates. Our goal was to observe the cell shape change with time. In other works, the cell capture efficiency has already been reported with a

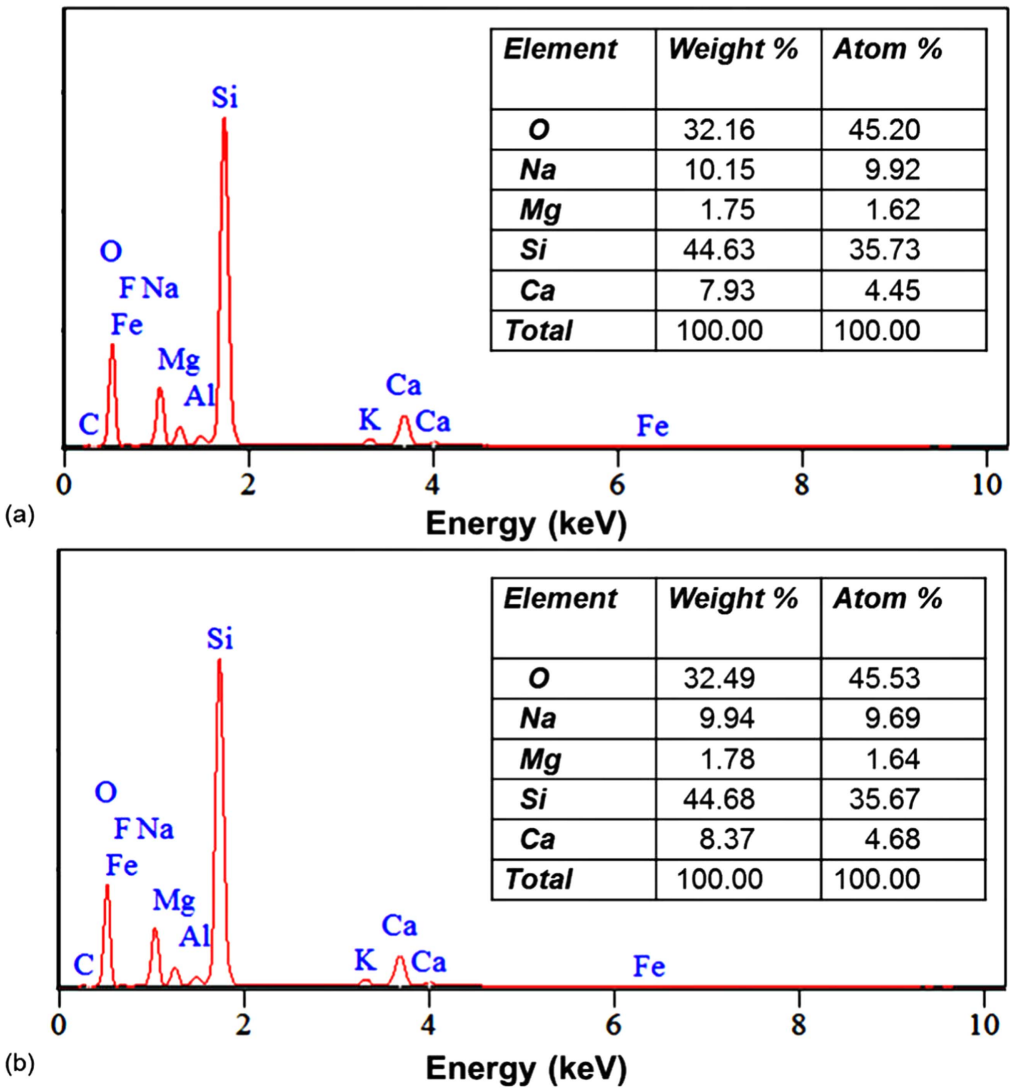

Figure 2. EDS analysis of (a) plane and (b) nanotextured glass substrates before chemical and biological modifications.

Table 2. Contact Angle Measurements (n = 7).

Substrate	Contact Angle ± S.D.
Plane	25° ± 1.5
Nanotextured	12° ± 1

washing step [9]. Standard cell incubation and washing requires a minimum of a 30 min period [9]. The reported morphological changes observed and reported here occurred within 30 min after incubation. The strength of the presented work is that no washing is required. There were some cells that were not bound to the substrates. During the observation of the bound cells, the unbound cells could be seen moving around in the suspension. The microscope objective was focused on the substrate so all the unbound cells were out of focus. The unbound and bound cells could be differentiated very clearly visually. The out of focus unbound cells were neither tracked nor their distance values were measured.

Cells captured on plane and nanotextured substrates were imaged for 15 min. Binary images of the cells were extracted from the optical images. Figure 3 shows representative cell behaviors observed in the images. Each panel shows one cell at a time, imaged at intervals of 3 min going from left to right. The data clearly shows that the non-metastatic cells (figures 3(c) and (d)) captured on plane and nanotextured substrates did not show a significant shape change. Metastatic cells changed their shapes more prominently on the nanotextured substrates (figure 3(a)) than on the plane substrates (figure 3(b)).

Prominent morphological changes of metastatic cells on anti-EGFR aptamer modified nanotextured substrates can be linked to the overexpression of EGFR on cell membrane. EGFRs of cell membrane are activated when captured on nanotextured substrates with anti-EGFR aptamers. Activated EGFR triggers PLCγ, an enzyme dependent intracellular signaling pathway, which influences cell motility [40–42]. Studies have also shown that this stimulation releases actin-modifying proteins from the cell membrane which reorganizes actin

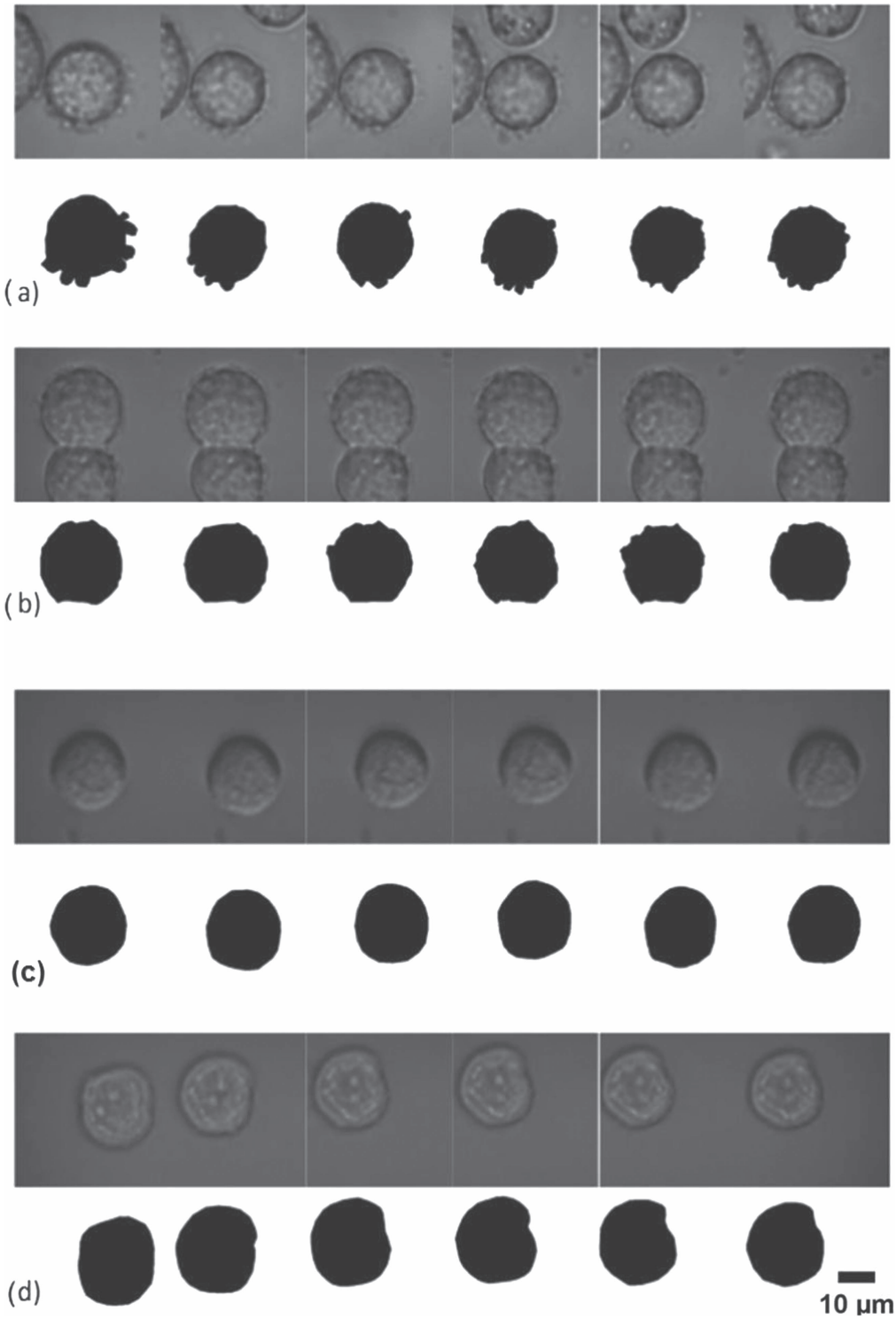

Figure 3. Cell behavior over 15 min. Going from left to right, each consecutive image is taken at 3 min intervals. The optical and binary images of (a) a metastatic cell captured on the nanotextured substrate; (b) a metastatic cell captured on the plane substrate; (c) a non-metastatic cell captured on the nanotextured substrate; and (d) a non-metastatic cell captured on the plane substrate.

cytoskeleton [43]. Actin cytoskeleton controls filopodia/lamellipodia extension and retraction in cells. Cells probe their surroundings with filopodia/lamellipodia. These are micron scale sheet-like structures made of actin mesh [44, 45]. In the presence of suitable/unsuitable binding sites on nanotextured substrates, filopodia/lamillipodia extend and retract. Through a microscope, this activity looks like contour changes of cells. The combined effect of increased anti-EGFR-aptamer density on nanotextured substrates and the overexpression of EGFR on metastatic cells ensues amplified morphological change of cells. Much is still unknown about the exact mechanisms and signaling pathways behind this shape change. The morphology change measurement has the potential to detect the finer detailed progression of non-metastatic cells as these become

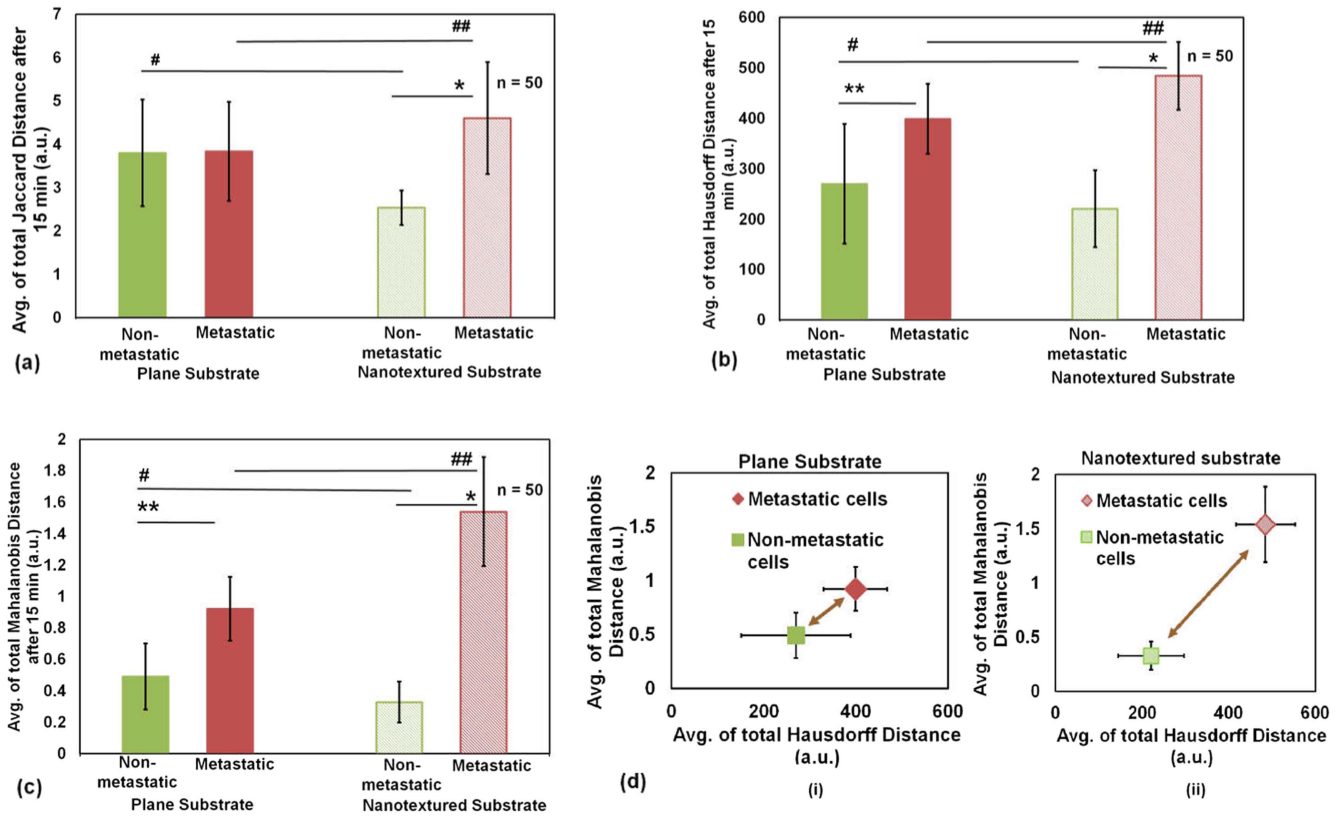

Figure 4. (a) Jaccard distance shows dissimilarity from the shape change of non-metastatic and metastatic cells on plane and nanotextured substrates (from two-tailed *t*-test, $^{*}p$-value < 0.0001; $^{\#}p$-value $= 0.02$; $^{\#\#}p$-value $= 0.2$); (b) Hausdorff distance analysis for shape dissimilarity analysis of the cells (from two-tailed *t*-test, $^{*}p$-value < 0.0001; $^{**}p$-value $= 0.0007$; $^{\#}p$-value $= 0.2$; $^{\#\#}p$-value $= 0.006$); (c) Mahalanobis distance analysis shows dissimilarity in the shape of the cells (from two-tailed *t*-test, $^{*}p$-value < 0.0001; $^{**}p$-value $= 0.001$; $^{\#}p$-value $= 0.02$; $^{\#\#}p$-value $= 0.0003$); (d) distance profiles of metastatic and non-metastatic cells on (i) plane and (ii) nanotextured substrate. Nanotexturing increases the propensity of metastatic cell shape change and induces higher changes in distance profile. The arrows show contrast between metastatic and non-metastatic cells. Detection efficiency increases for metastatic cells on anti-EGFR aptamer modified nanotextured substrates.

metastatic. In the presented work, we see a snapshot of the two cell conditions and further work with varied cell over-expression can provide metrics on the limit of detection of the presented approach.

Here, we detected the shape change of cells from optical images and converted these changes into numeric values to objectively differentiate between metastatic and non-metastatic cells.

3.5. Distance matrix analysis: Jaccard distance

For higher dissimilarity in shape, the Jaccard distance has higher values. A sensitive detection platform is capable of rendering statistically significant values using simple operations. The Jaccard distance value gives a clear measure of the sensitivity of nanotextured functionalized substrates in distinguishing between metastatic and non-metastatic cells. In figure 4(a), we see that on plane substrates, the Jaccard distance does not show difference between metastatic and non-metastatic cells (both averages ~3.8 a.u.; both S.D.s ~1.2 a.u.). But on nanotextured substrates, the disparity is statistically significant and metastatic cells are easily distinguishable ($^{*}p$-value < 0.001). The average for metastatic cells is 4.6 a.u. (S.D. = 1.2 a.u.) and non-metastatic cells is 2.5 a.u. (S.D. = 0.39 a.u.) on the nanotextured substrate. The non-metastatic to metastatic cell shape change ratio jumped from 1:1.01 to 1:1.81 for the Jaccard distance from plane to nanotextured substrates. Evidently, nanotextured anti-EGFR aptamer modified substrates are remarkably more sensitive in detecting metastatic cells from non-metastatic cells than plane functionalized substrates. This shows the compound effect of aptamer interactions and nanotexture.

Overactive extension and retraction of cell membrane for metastatic cells captured on anti-EGFR aptamer modified nanotextured substrates resulted in a higher Jaccard distance value than that for non-metastatic cells. Metastatic cells are more flexible than benign cells because of their cytoskeleton structure [46–48]. The agility of actin cytoskeleton structure is thus the vital component in defining vigorous cell membrane extension/retraction of metastatic cells [49, 50].

3.6. Distance matrix analysis: Hausdorff distance

Hausdorff distance calculation is fast, simple, and tolerant of positional errors. This distance value is very rigorous and precise in calculating small positional changes. If cells do not change shape, the Hausdorff distance value is very low and vice versa. In figure 4(b), the averages of total Hausdorff distance changes for cells are plotted. On the plane substrates,

the metastatic cells shows a higher Hausdorff distance; i.e. higher dissimilarity than non-metastatic cells ($^{**}p$-value < 0.05). The distance value is larger because the metastatic cells were rapidly changing shape. On nanotextured substrates, the difference between the distance values of metastatic and non-metastatic cells is even higher ($^{*}p$-value < 0.0001). The average of the total distance for non-metastatic cells decreases from 270.4 a.u. (S.D. = 118.5 a.u.) to 220.8 a.u. (S.D. = 76.25 a.u.) going from plane to nanotextured substrates. An opposite effect can be seen on metastatic cells as the average of the total Hausdorff distance increases from 399.1 a.u. (S.D. = 69.3 a.u.) to 484.7 a.u. (S.D. = 67.7 a.u.) going from plane to nanotextured substrates. Nanotexture significantly enhanced the activity of metastatic cells while it suppressed the activity of non-metastatic cells. As metastatic cells had more EGFR on the cell membranes, these became vigorously active to create more bonds with high density aptamer molecules functionalized on the nanotextured substrates. The non-metastatic cells with a low density of EGFR on the cell membrane became inactive precisely for the same reason. The non-metastatic to metastatic cell shape change ratio improved from 1:1.48 to 1:2.19 for the Hausdorff distance analysis going from plane to nanotextured substrates. Undoubtedly, nanotexturing did increase the possibility of detecting metastatic breast cancer cells on anti-EGFR aptamer functionalized substrates.

3.7. Distance matrix analysis: Mahalanobis distance

The Mahalanobis distance of a changing cell boundary was calculated. A larger Mahalanobis distance meant a larger change in cell boundary. This is evident from figure 4(c). The distinguishing factor between metastatic and non-metastatic cells is the difference in their respective average distances. On plane substrates, the average distances are 0.49 a.u. (S.D. = 0.21 a.u.) and 0.92 a.u. (S.D. = 0.2 a.u.) for non-metastatic and metastatic cells, respectively ($^{**}p$-value $<$ 0.05). On nanotextured substrates, the statistical significance is enhanced, going from 0.32 a.u. (S.D. = 0.13 a.u.) to 1.53 a.u. (S.D. = 0.34 a.u.) for non-metastatic to metastatic cells ($^{*}p$-value < 0.0001). Nanotexture amplified the morphology change of metastatic cells to such an extent that Mahalanobis distance analysis clearly differentiated between the behavior of metastatic cells on plane and nanotextured substrates ($^{\#\#}p$-value = 0.0003). The non-metastatic to metastatic cell shape change ratio improved from 1:1.87 to 1:4.69 for Mahalanobis distance analysis going from plane to nanotextured substrates.

Nanotexture increased the cell shape alteration frequency for metastatic cells. The reason is the overexpression of EGFR on a metastatic cell membrane, which is 10 times higher than on non-metastatic cells [28]. Stimulated EGFR has been reported to cause cell proliferation and migration [51]. Cell movement begins in response to external signals detected by receptors like EGFR [52]. On nanotextured substrates, the higher density of anti-EGFR aptamer got bound with and activated overexpressed EGFR on metastatic cell membrane prompting cascades of intracellular signals. This stimulation resulted in continuous restructuring of actin filaments [53]. Hence, the cytoskeleton structure of metastatic cells was more dynamic on nanotextured substrates than on plane substrates. In figure 4(d), we can see metastatic cells on plane and nanotextured substrates behave significantly different in terms of cell morphology. On the nanotexture, high frequency morphology change of these cells enable our functionalized platform to effectively differentiate between metastatic and non-metastatic cells.

In figure 4(d), the distance profiles for metastatic and non-metastatic cells are summarized to show the enhancement in contrast. Hausdorff and Mahalanobis distances are plotted here, but the Jaccard distance can be included as well. Distance profiles on plane substrates (figure 4(d-i)) and on nanotextured substrates (figure 4(d-ii)) are shown. It is evident that the differentiation between metastatic and non-metastatic cells is amplified on nanotextured anti-EGFR aptamer modified substrate. The change going from figure 4(d-i) to figure 4(d-ii) brings to light another important aspect of biomarker overexpression. In patient samples, the distance profiles (reflecting intermediary cells undergoing EMT) overlap due to the possibility of cells that are not yet metastatic. This may be the reason that both types of cells overlap in the distance space. Visually, for the nanotextured substrate, the cutoff is approximately at the average of the total Hausdorff distance (350 a.u.) and the average of the total Mahalanobis distance (1 a.u.). We may be able to increase the resolution of detection and thus clearly define the crossover boundary for cell types using multiple known biomarkers and using knowledge of their overexpression.

The Hausdorff distance is very critical to positional change and takes very minute changes into account. On the other hand, the Mahalanobis distance deals with covariance between changing cell boundaries. It is much more flexible and disregards subtle changes. Cells are live entities and sometimes show very small morphological changes with time. The Mahalanobis distance is very handy to compute shape change in this regard. But at the same time precision is needed and it is provided by the Hausdorff distance. Therefore, plotting these two distances together combines precision and flexibility, and establishes distance profiles for metastatic and non-metastatic cells.

As stated before, another advantage of nanotextured substrate over plane substrate is that it has effectively more surface area [19]. Hence, a greater number of linker ssDNA and thus RNA aptamer molecules are tethered on nanotextured substrates. Capture efficiency has already been reported to go up for cancer cells on nanotextured substrates [19]. There is thus more to nanotexture than just surface area. In this work, the shape change phenomena of cancer cells on aptamer modified nanotextured substrates has been investigated and quantifiable differentiation metrics have been defined to objectively categorize metastatic cells from non-metastatic ones.

Distinguishing metastatic cells from non-metastatic ones is critical for cancer staging to define an appropriate treatment regime. The fabrication process for the glass substrate is easy, economical, and scalable. The capture process is selective, efficient, and label-free [9]. The aptamer modified nanotextured

platform enhances cell motility which is a novel and easy physical biomarker for early detection. Established distance profiles for metastatic and non-metastatic cells provide simple metrics for objective and error-free differentiation. Overall, the implementation of a nanotextured functionalized platform with optical image analysis yielded an innovative strategy for sensing metastatic breast cancer cells in a simple and economical setting.

4. Conclusions

Early detection of metastatic breast cancer is important for effective therapy and reduced mortality rates. The main challenge is to distinguish metastatic cells from non-metastatic ones. This work presented a nanotextured platform and analysis approaches for rapid, robust, and objective detection of metastatic cells from non-metastatic ones. The results demonstrated that aptamer modified nanotextured substrates substantially enhanced the morphological changes of captured metastatic cells. This physical attribute can be used as a cellular biomarker for metastatic cancer cell detection. The quantification produced a statistically significant difference between metastatic and non-metastatic cell features. Functionalized nanotextured substrates integrated with the image processing and analysis methods can thus be incorporated in effective point-of-care devices for affordable and quick detection of metastatic breast cancer.

Acknowledgments

We would like to thank Dr Andrew D Ellington of the University of Texas at Austin for providing the anti-EGFR aptamer, Dr Mohammed Arif I Mahmood for technical help, Dr Loan Bui for assistance in cell handling, and the staff of the Nanotechnology Research Center for the training on the equipment. This work was supported by the National Science Foundation under grant number ECCS- 1407990.

ORCID iDs

Samir M Iqbal https://orcid.org/0000-0002-3764-1405

References

[1] McGuire S 2016 World Cancer Report 2014. Geneva, Switzerland: World Health Organization, International Agency for Research on Cancer, WHO Press, 2015. *Adv. Nutr.* **7** 418–9
[2] Chambers A F, Groom A C and MacDonald I C 2002 Metastasis: dissemination and growth of cancer cells in metastatic sites *Nat. Rev. Cancer* **2** 563–72
[3] Fidler I J 2003 The pathogenesis of cancer metastasis: the'seed and soil'hypothesis revisited *Nat. Rev. Cancer* **3** 453–8
[4] Weigelt B, Peterse J L and Van't Veer L J 2005 Breast cancer metastasis: markers and models *Nat. Rev. Cancer* **5** 591–602
[5] Nagrath S *et al* 2007 Isolation of rare circulating tumour cells in cancer patients by microchip technology *Nature* **450** 1235–9
[6] Adams A A *et al* 2008 Highly efficient circulating tumor cell isolation from whole blood and label-free enumeration using polymer-based microfluidics with an integrated conductivity sensor *J. Am. Chem. Soc.* **130** 8633–41
[7] Tan S J *et al* 2009 Microdevice for the isolation and enumeration of cancer cells from blood *Biomed. Microdevices* **11** 883–92
[8] Swennenhuis J F *et al* 2009 Characterization of circulating tumor cells by fluorescence *in situ* hybridization *Cytometry Part* A **75** 520–7
[9] Wan Y *et al* 2010 Surface-immobilized aptamers for cancer cell isolation and microscopic cytology *Cancer Res* **70** 9371–80
[10] Bunka D H and Stockley P G 2006 Aptamers come of age–at last *Nat. Rev. Microbiol.* **4** 588–96
[11] Sullenger B A and Gilboa E 2002 Emerging clinical applications of RNA *Nature* **418** 252–8
[12] Liliensiek S J, Nealey P and Murphy C J 2009 Characterization of endothelial basement membrane nanotopography in rhesus macaque as a guide for vessel tissue engineering *Tissue Eng. Part* A **15** 2643–51
[13] Liotta L *et al* 1980 Metastatic potential correlates with enzymatic degradation of basement membrane collagen *Nature* **284** 67–8
[14] Fischer K E *et al* 2009 Biomimetic nanowire coatings for next generation adhesive drug delivery systems *Nano Lett.* **9** 716–20
[15] Kim S T *et al* 2010 Novel streptavidin-functionalized silicon nanowire arrays for CD4+ T lymphocyte separation *Nano Lett.* **10** 2877–83
[16] Asghar W *et al* 2012 Synthesis of nano-textured biocompatible scaffolds from chicken eggshells *Nanotechnology* **23** 475601
[17] Thapa A *et al* 2003 Nano-structured polymers enhance bladder smooth muscle cell function *Biomaterials* **24** 2915–26
[18] Miller D C *et al* 2004 Endothelial and vascular smooth muscle cell function on poly (lactic-co-glycolic acid) with nano-structured surface features *Biomaterials* **25** 53–61
[19] Wan Y *et al* 2012 Nanotextured substrates with immobilized aptamers for cancer cell isolation and cytology *Cancer* **118** 1145–54
[20] Mahmood M A I *et al* 2014 Micro+ nanotexturing of substrates to enhance ligand-assisted cancer cell isolation *Nanotechnology* **25** 475102
[21] Islam M *et al* 2015 Effects of nanotexture on electrical profiling of single tumor cell and detection of cancer from blood in microfluidic channels *Sci. Rep.* **5** 13031
[22] Islam M *et al* 2016 Electrical profiling and aptamer functionalized nanotextured surface in a single biochip for the detection of tumor cells *Func. Nanostructures* **1** 13–21
[23] Mahmood M A I *et al* 2015 One-step tumor detection from dynamic morphology tracking on aptamer-grafted surfaces *Technology* **3** 194–200
[24] Mendelsohn J 2004 EGF receptors as a target for cancer therapy *Trans. Am. Clin. Climatol. Assoc.* **115** 249
[25] Maheswaran S *et al* 2008 Detection of mutations in EGFR in circulating lung-cancer cells *N. Engl. J. Med.* **359** 366–77
[26] Franovic A *et al* 2007 Translational up-regulation of the EGFR by tumor hypoxia provides a nonmutational explanation for its overexpression in human cancer *Proc. Natl. Acad. Sci.* **104** 13092–7
[27] Carpenter G and Cohen S 1979 Epidermal growth factor *Ann. Rev. Biochem.* **48** 193–216
[28] Cai Z *et al* 2008 Relationship between induction of phosphorylated H2AX and survival in breast cancer cells exposed to 111In-DTPA-hEGF *J. Nucl. Med.* **49** 1353–61

[29] Osborne S E, Matsumura I and Ellington A D 1997 Aptamers as therapeutic and diagnostic reagents: problems and prospects *Curr. Opin. Chem. Biol.* **1** 5–9
[30] Jaccard P 1901 Distribution de la flore alpine dans le Bassin des Dranses et dans quelques régions voisines *Bull. Soc. Vaud. Sci. Nat.* **37** 241–72
[31] Huttenlocher D P, Klanderman G A and Rucklidge W J 1993 Comparing images using the Hausdorff distance *IEEE Trans. Pattern Anal. Mach. Intell.* **15** 850–63
[32] Mahalanobis P C 1936 On the generalized distance in statistics *Proc. Nat. Inst. Sci. (Calcutta)* **2** 49–55
[33] Nosonovsky M and Bhushan B 2008 Biologically inspired surfaces: broadening the scope of roughness *Adv. Funct. Mater.* **18** 843–55
[34] Scotchford C A *et al* 2002 Protein adsorption and human osteoblast-like cell attachment and growth on alkylthiol on gold self-assembled monolayers *J. Biomed. Mater. Res.* **59** 84–99
[35] Ferretti S *et al* 2000 Self-assembled monolayers: a versatile tool for the formulation of bio-surfaces *TRAC Trends Anal. Chem.* **19** 530–40
[36] John P M S *et al* 1997 Preferential glial cell attachment to microcontact printed surfaces *J. Neurosci. Methods* **75** 171–7
[37] Zreiqat H and Howlett C R 1999 Titanium substrata composition influences osteoblastic phenotype: *in vitro* study *J. Biomed. Mater. Res.* **47** 360–6
[38] Zreiqat H, Evans P and Howlett C R 1999 Effect of surface chemical modification of bioceramic on phenotype of human bone-derived cells *J. Biomed. Mater. Res. Part* A **44** 389–96
[39] Healy K E *et al* 1996 Kinetics of bone cell organization and mineralization on materials with patterned surface chemistry *Biomaterials* **17** 195–208
[40] Chen P *et al* 1994 Epidermal growth factor receptor-mediated cell motility: phospholipase C activity is required, but mitogen-activated protein kinase activity is not sufficient for induced cell movement *J. Cell Biol.* **127** 847–57
[41] Chen P, Gupta K and Wells A 1994 Cell movement elicited by epidermal growth factor receptor requires kinase and autophosphorylation but is separable from mitogenesis *J. Cell Biol.* **124** 547–55
[42] Chen P, Murphy-Ullrich J E and Wells A 1996 A role for gelsolin in actuating epidermal growth factor receptor-mediated cell motility *J. Cell Biol.* **134** 689–98
[43] Van Leeuwen F N *et al* 1999 Rac regulates phosphorylation of the myosin-II heavy chain, actinomyosin disassembly and cell spreading *Nat. Cell Biol.* **1** 242–8
[44] Anselme K 2000 Osteoblast adhesion on biomaterials *Biomaterials* **21** 667–81
[45] Mogilner A and Oster G 1996 Cell motility driven by actin polymerization *Biophys. J.* **71** 3030–45
[46] Suresh S, Mills J and Dao M 2005 Single-cell nanomechanics and human disease states *Abstr. Pap. Am. Chem. Soc.* **230** U1092
[47] Guck J *et al* 2005 Optical deformability as an inherent cell marker for testing malignant transformation and metastatic competence *Biophys. J.* **88** 3689–98
[48] Suresh S 2007 Biomechanics and biophysics of cancer cells *Acta Mater.* **55** 3989–4014
[49] Betz T, Lim D and Käs J A 2006 Neuronal growth: a bistable stochastic process *Phys. Rev. Lett.* **96** 098103
[50] Hofman P *et al* 1999 Neutrophil F-actin and myosin but not microtubules functionally regulate transepithelial migration induced by interleukin 8 across a cultured intestinal epithelial monolayer *Eur. Cytokine Network* **10** 227–36
[51] Wells A 1999 EGF receptor *Int. J. Biochem. Cell Biol.* **31** 637–43
[52] Alberts B *et al* 2002 *Molecular Biology of the Cell* 4th edn (London: Garland Science, Taylor and Francis)
[53] Parent C A and Devreotes P N 1999 A cell's sense of direction *Science* **284** 765–70